Nafion/Zeolite Nanocomposite Membrane by in Situ Crystallization for a Direct Methanol Fuel Cell

Zhongwei Chen,[†] Brett Holmberg,[†] Wenzhen Li,[†] Xin Wang,[†] Weiqiao Deng,[†,‡] Ronnie Munoz,[†] and Yushan Yan*[,†]

Department of Chemical and Environmental Engineering, Bourns College of Engineering, Center for Environmental Research and Technology (CE-CERT), University of California−Riverside, Riverside, California 92521, and Materials and Process Simulation Center, California Institute of Technology, Pasadena, California 91125

Received April 12, 2006. Revised Manuscript Received September 11, 2006

A method for preparing Nafion/acid functionalized zeolite Beta (NAFB) nanocomposite membranes by in situ hydrothermal crystallization is described. The nanocomposite membranes have a slightly lower proton conductivity but a markedly lower methanol permeability (ca. 40% reduction). When tested with 1 M methanol feed, the direct methanol fuel cells (DMFCs) with the NAFB composite membranes have a slightly higher open circuit voltage (OCV; 3%) and much higher maximum power density (21%) than those with the pure Nafion 115 membranes. With a higher methanol concentration (5 M), the DMFCs with the NAFB composite membranes demonstrate a 14% higher OCV and a 93% higher maximum power density than those with the pure Nafion 115 membranes. Compared with the commercial Nafion 115 membranes, the NAFB composite membranes have slightly lower tensile strength but higher elastic modulus.

1. Introduction

Direct methanol fuel cells (DMFCs) are one of the most attractive power sources for portable electronics, due to their system simplicity and their use of high-energy density liquid fuel, methanol.[1−3] Polyperfluorosulfonic acid ionomer developed by Dupont, under the trademark of Nafion, is the most commonly used proton exchange membrane for DMFCs because of its excellent chemical stability and high proton conductivity. However, Nafion membrane has high methanol permeability, commonly referred to as methanol crossover, because methanol is easily transported together with the solvated protons through the water-filled ion cluster channels within Nafion structure.[4,5] This methanol crossover from anode to cathode is one of the major problems hampering practical applications of DMFCs, because it wastes the fuel and causes performance losses at the cathode due to the mixed potential effect and catalyst poisoning.[4−7]

Recent literature describes the modifications of Nafion membranes by a variety of organic and inorganic materials such as silicon oxide,[8,9] zirconia,[10,11] titania,[12] alumina,[13] zirconium phosphates,[14] Pd,[15] polypyrrole,[16] polyfurfuryl alcohol,[17] and polyoxyalkylenes.[18] Nafion−inorganic filler composite membranes mainly have been prepared via two methods: (i) mixing Nafion solutions with inorganic fillers or their precursors followed by casting[8−10,12−14,19] and (ii) infiltration of commercial Nafion membranes with precursors of inorganic fillers.[11,15−17] Nafion is composed of discrete hydrophobic and hydrophilic regions.[20] The hydrophobic region is the polymer fluorocarbon backbone. The hydrophilic region contains the ionic groups and their counter ions which form the ionic clusters and the inter-cluster channels

* Corresponding author. Fax: 1-951-827-5696. Tel.: 1-951-827-2068. E-mail: yushan.yan@ucr.edu.
[†] University of CaliforniasRiverside.
[‡] California Institute of Technology.

(1) McNicol, B. D.; Rand, D. A. J.; Williams, K. R. *J. Power Sources* **1999**, *83*, 15−31.
(2) Ren, X.; Zelenay, P.; Thomas, S.; Davey, J.; Gottesfeld, S. *J. Power Sources* **2000**, *86*, 111−116.
(3) Dillon, R.; Srinivasan, S.; Arico, A. S.; Antonucci, V. In *J. Power Sources*, Eight Ulmer Electrochemische Tage, Neu-Ulm, Germany, June 2002; Garche, J., Gutmann, G., Eds.; Elsevier: New York, 2004; Vol. 127, issue 1−2, pp 112−126.
(4) Ravikumar, M. K.; Shukla, A. K. *J. Electrochem. Soc.* **1996**, *143*, 2601−2606.
(5) Heinzel, A.; Barragan, V. M. *J. Power Sources* **1999**, *84*, 70−74.
(6) Scott, K.; Taama, W. M.; Argyropoulos, P.; Sundmacher, K. *J. Power Sources* **1999**, *83*, 204−216.
(7) Gurau, B.; Smotkin, E. S. *J. Power Sources* **2002**, *112*, 339−352.
(8) Wang, H. T.; Holmberg, B. A.; Huang, L. M.; Wang, Z. B.; Mitra, A.; Norbeck, J. M.; Yan, Y. S. *J. Mater. Chem.* **2002**, *12*, 834−837.
(9) Shao, Z. G.; Joghee, P.; Hsing, I. M. *J. Membr. Sci.* **2004**, *229*, 43−51.
(10) Ruffmann, B.; Silva, H.; Schulte, B.; Nunes, S. P. In *Solid State Ionics*, Proceedings of the Eleventh International Conference on Solid State Protonic Conductors, Guildford, U.K., August 2002; Slade, R. C. T., Varcoe, J. R., Eds.; Elsevier: New York, 2003; Vol. 162−163, pp 269−275.
(11) Choi, P.; Jalani, N. H.; Datta, R. *J. Electrochem. Soc.* **2005**, *152*, A1548−A1554.
(12) Watanabe, M.; Uchida, H.; Emori, M. *J. Phys. Chem. B* **1998**, *102*, 3129−3137.
(13) Arico, A. S.; Baglio, V.; Di Blasi, A.; Creti, P.; Antonucci, P. L.; Antonucci, V. *Solid State Ionics* **2003**, *161*, 251−265.
(14) Yang, C.; Srinivasan, S.; Bocarsly, A. B.; Tulyani, S.; Benziger, J. B. *J. Membr. Sci.* **2004**, *237*, 145−161.
(15) Kim, Y.-M.; Park, K.-W.; Choi, J.-H.; Park, I.-S.; Sung, Y.-E. *Electrochem. Commun.* **2003**, *5*, 571−574.
(16) Easton, E. B.; Langsdorf, B. L.; Hughes, J. A.; Sultan, J.; Qi, Z.; Kaufman, A.; Pickup, P. G. *J. Electrochem. Soc.* **2003**, *150*, C735−C739.
(17) Liu, J.; Wang, H.; Cheng, S.; Chan, K.-Y. *Chem. Commun.* **2004**, 728−729.
(18) Malhotra, S.; Datta, R. *J. Electrochem. Soc.* **1997**, *144*, L23−L26.
(19) Aparicio, M.; Klein, L. C. *J. Electrochem. Soc.* **2005**, *152*, A493−A496.
(20) Mauritz, K. A.; Moore, R. B. *Chem. Rev.* **2004**, *104*, 4535−4585.

10.1021/cm060841q CCC: $33.50
Published on Web 11/07/2006

in the Nafion.[20] For the infiltration method, the hydrophilic ionic clusters and the inter-cluster channels of Nafion were used as a template or a reaction vessel for the formation of the inorganic phases such as silicon oxide,[21−24] zirconium phosphate,[14] and ORMOSIL.[25−31] These composite membranes containing inorganic fillers indeed reduced the methanol crossover, but this effect did not always lead to a desired improvement in the performance of the membrane−electrode assemblies (MEAs), mainly because the proton conductivity of the composite membranes was often markedly lower than that of the pure Nafion membranes.

Zeolites, a class of crystalline aluminosilicates, are proton conducting, hygroscopic, and microporous materials and have been used as inorganic fillers in composite membranes by employing a casting method. Most zeolites used in the composite membranes for fuel cells in the literature are micrometer-sized particles with low proton conductivity.[32−35] Nanometer-sized inorganic additives have proved to be crucial to the compatibility between the inorganic filler and Nafion, which has significant effects on the proton conductivity and methanol permeability of the composite membranes.[36] Different types of zeolite nanocrystals (A, NaX, NaY, Beta, etc.) have been prepared successfully by template and template-free methods in our group.[37−45] To minimize the loss of proton conductivity caused by the fillers while reducing the methanol permeability, acid functionalized zeolites have been prepared[46] and used successfully as an inorganic filler in composite membranes in our previous work.[42] The acid functionalized zeolites were selected for their good proton conductivity (∼0.02 S/cm), excellent acid stability, and hydrophilic nature. The particle size of the acid functionalized Beta (AFB) nanocrystals was still larger than 50 nm, and there was aggregation between the AFB nanocrystals during the composite membrane casting. The performance improvements of the composite membranes were sometimes limited, likely because the recast Nafion membranes had a significantly different microstructure from the commercial thermally processed Nafion membrane.[45]

Recently, we sought to take advantage of the unique structure offered by the commercial thermally processed Nafion membranes and developed an in situ crystallization process to fabricate Nafion/AFB (NAFB) nanocomposite membranes by the following steps: (1) impregnation of a Nafion membrane in the precursor solution for the organic functionalized Beta synthesis; (2) hydrothermal treatment of the impregnated Nafion membrane in the synthesis solution to grow organic functionalized Beta nanocrystals inside the Nafion membrane; and (3) concentrated H_2SO_4 solution treatment to remove the template in the zeolite pores and at the same time sulfonate the organic functional groups. Here the hydrophilic ionic clusters of the Nafion membrane likely served as the nanoreactors for the formation of the functionalized Beta nanocrystals. The main advantages of this method are as follows: (i) smaller AFB nanocrystals, without agglomeration, are formed in the ionic clusters of the Nafion membrane (Figure 1a); (ii) the embedded AFB nanocrystals have the ability to reduce the methanol crossover, while still allowing proton transport via the acid groups present in their internal pores and on their external surfaces (Figure 1b); and (iii) the Nafion polymer host still has the same microstructure as the commercial thermally processed Nafion membrane. To the best of our knowledge, this is the first time that Nafion/nanozeolite composite membranes have been produced by an in situ crystallization method.

2. Experimental Section

2.1. Preparation of Precursor Solution of Organic Functionalized Beta. The synthesis solution was prepared as follows.[42] Two precursor solutions, one with aluminum and the other containing silica, were prepared for each batch reaction. The aluminum precursor solution was composed of Al powder (99.95%, Al, Aldrich) and half of the required tetraethyl ammonium hydroxide (TEAOH; 35 wt % in water, SACHEM). The silica precursor solution was composed of the remaining half of the recipe's TEAOH, double deionized (DDI) H_2O, fumed SiO_2 (99.8 wt %, Aldrich), and phenethyltrimethoxysilane (PETMS; 99.8%, Aldrich). Both solutions were stirred vigorously until the aluminum solution became clear, indicating the complete reaction of the aluminum powder. Finally, the solutions were mixed together in one bottle for 3 h at room temperature. The molar composition of the synthesis solution was 1.0:48.5:1.5:14:750 Al_2O_3/SiO_2 (fumed)/SiO_2 (PETMS)/$(TEA)_2O$ ($2OH^-$)/H_2O. The weight composition of a typical batch was 20.00 g of TEAOH, 0.0917 g of aluminum powder, 4.97 g of fumed SiO_2, 9.94 g of DDI H_2O, and 0.55 g of PETMS.

(21) Adjemian, K. T.; Srinivasan, S.; Benziger, J.; Bocarsly, A. B. *J. Power Sources* **2002**, *109*, 356−364.
(22) Baradie, B.; Dodelet, J. P.; Guay, D. *J. Electroanal. Chem.* **2000**, *489*, 101−105.
(23) Miyake, N.; Wainright, J. S.; Savinell, R. F. *J. Electrochem. Soc.* **2001**, *148*, A898−A904.
(24) Miyake, N.; Wainright, J. S.; Savinell, R. F. *J. Electrochem. Soc.* **2001**, *148*, A905−a909.
(25) Mauritz, K. A. *Mater. Sci. Eng., C* **1998**, *6*, 121−133.
(26) Deng, Q.; Cable, K. M.; Moore, R. B.; Mauritz, K. A. *J. Polym. Sci., Part B: Polym. Phys.* **1996**, *34*, 1917−1923.
(27) Deng, Q.; Hu, Y.; Moore, R. B.; McCormick, C. L.; Mauritz, K. A. *Chem. Mater.* **1997**, *9*, 36−44.
(28) Deng, Q.; Jarrett, W.; Moore, R. B.; Mauritz, K. A. *J. Sol.-Gel Sci. Technol.* **1996**, *7*, 177−190.
(29) Deng, Q.; Moore, R. B.; Mauritz, K. A. *Chem. Mater.* **1995**, *7*, 2259−2268.
(30) Deng, Q.; Wilkie, C. A.; Moore, R. B.; Mauritz, K. A. *Polymer* **1998**, *39*, 5961−5972.
(31) Young, S. K.; Jarrett, W. L.; Mauritz, K. A. *Polymer* **2002**, *43*, 2311−2320.
(32) Tricoli, V.; Nannetti, F. *Electrochim. Acta* **2003**, *48*, 2625−2633.
(33) Libby, B.; Smyrl, W. H.; Cussler, E. L. *AIChE J.* **2003**, *49*, 991−1001.
(34) Baglio, V.; Di, Blasi, A.; Arico, A. S.; Antonucci, V.; Antonucci, P. L.; Nannetti, F.; Tricoli, V. *Electrochim. Acta* **2005**, *50*, 5181−5188.
(35) Rhee, C. H.; Kim, H. K.; Chang, H.; Lee, J. S. *Chem. Mater.* **2005**, *17*, 1691−1697.
(36) Zimmerman, C. M.; Singh, A.; Koros, W. J. *J. Membr. Sci.* **1997**, *137*, 145−154.
(37) Chen, Z. W.; Li, S.; Yan, Y. S. *Chem. Mater.* **2005**, *17*, 2262−2266.
(38) Chen, Z. W.; Li, S. A.; Yan, Y. S. *Abstracts Papers ACS* **2004**, *227*, U1296−U1296.
(39) Wang, H. T.; Holmberg, B. A.; Yan, Y. S. *J. Am. Chem. Soc.* **2003**, *125*, 9928−9929.
(40) Wang, H. T.; Huang, L. M.; Holmberg, B. A.; Yan, Y. S. *Chem. Commun.* **2002**, 1708−1709.
(41) Wang, H. T.; Holmberg, B. A.; Yan, Y. S. *J. Mater. Chem.* **2002**, *12*, 3640−3643.
(42) Holmberg, B. A.; Hwang, S. J.; Davis, M. E.; Yan, Y. S. *Microporous Mesoporous Mater.* **2005**, *80*, 347−356.
(43) Holmberg, B. A.; Wang, H.; Yan, Y. S. *Microporous Mesoporous Mater.* **2004**, *74*, 189−198.
(44) Holmberg, B. A.; Wang, H. T.; Norbeck, J. M.; Yan, Y. S. *Microporous Mesoporous Mater.* **2003**, *59*, 13−28.
(45) Holmberg, B. A.; Wang, X.; Norbeck, J. M.; Yan, Y. S. *Abstracts Papers ACS* **2004**, *227*, U407−U407.
(46) Jones, C. W.; Tsuji, K.; Davis, M. E. *Nature* **1998**, *393*, 52−54.

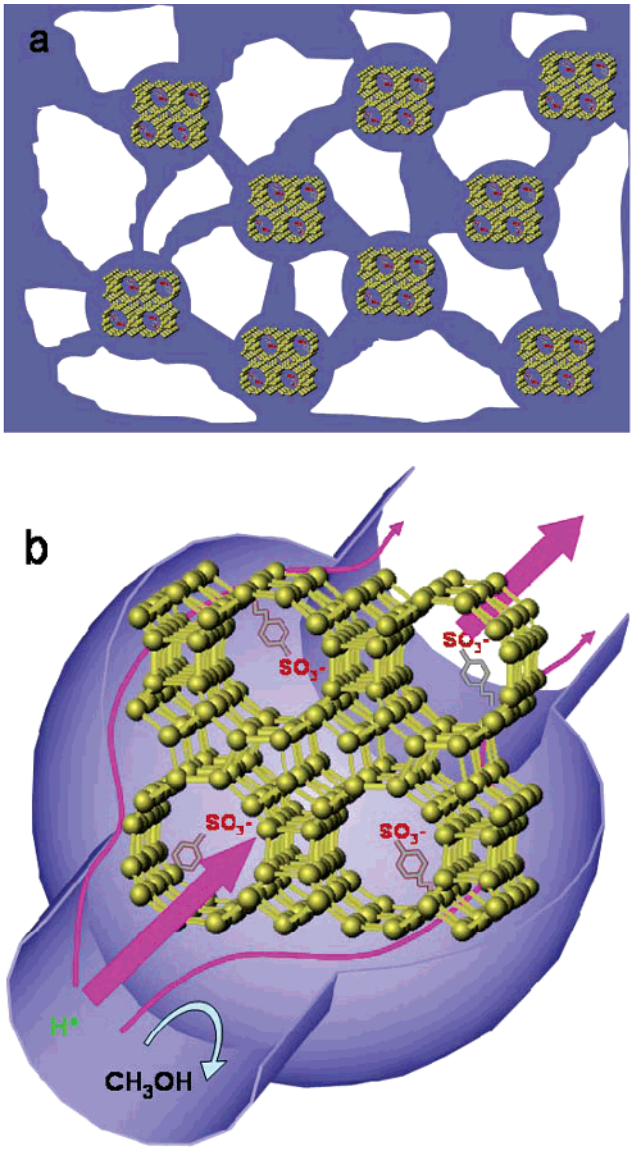

Figure 1. Schematics of NAFB composite membrane and its proton and methanol transport. (a) White region represents the hydrophobic section of the Nafion membrane, and the colored region represents the hydrophilic section of the Nafion membrane; (b) proton and methanol transport in the NAFB composite membrane.

2.2. Preparation of Composite Membrane. First, Nafion 115 membrane was boiled in a 3 wt % H_2O_2 solution for 1 h and then rinsed with boiling DDI H_2O. Second, it was boiled in a 0.5 M sulfuric acid solution for 1 h, followed by rinsing with boiling DDI H_2O. Third, the membrane was boiled for 1 h in DDI H_2O, allowed to cool, and kept in DDI water. Finally, it was swollen in a boiling methanol−water solution (1:1 (v/v)) to expand the membrane.

A Teflon liner with a volume of 45 mL was rinsed and scrubbed thoroughly with Alconox and DDI H_2O. Then about 35 mL of the organic functionalized Beta precursor solution was loaded, and the treated Nafion 115 membrane of the desired dimensions was immersed in the synthesis solution. The Teflon liner was then sealed inside a stainless steel autoclave. The autoclave was then inserted into our custom tumbling apparatus and tumbled end over end at 70 revolutions per minute (rpm) within a convection oven at room temperature for 1 day, followed at 140 °C for 7 days. The resulting composite membranes were treated in concentrated sulfuric acid (96 wt %) at 80 °C overnight. After that, they were treated with a commonly used pretreatment procedure using H_2O_2 and H_2SO_4 solutions described as follows. They were first boiled in 3 wt % H_2O_2 for 1 h and then rinsed with boiling DDI H_2O. Then, they were boiled in a 0.5 M sulfuric acid solution for 1 h, followed by rinsing with boiling DDI H_2O. Finally, the membranes were boiled for 1 h in DDI H_2O and allowed to cool, after which the membranes were ready for testing.

2.3. Characterizations. *X-ray Diffraction (XRD).* XRD patterns were obtained on a Bruker D8 Advance Diffractometer (Bruker AXS) using a Cu Kα radiation. The dried membranes were mounted on an aluminum sample holder. The scanning angle ranged from 5° to 50° with a scanning rate of 3° min^{-1}. All the spectra were taken at ambient conditions.

Scanning Electron Microscopy (SEM) and Energy Dispersive X-ray Spectroscopy (EDS). The morphologies of the surfaces and the cross-sections of the membranes were investigated with a Philips XL30-FEG scanning electron microscope. For the cross-sectional SEM samples, the membranes were freeze-fractured in liquid N_2. The EDS attachment of the microscope was used to analyze the chemical composition of the samples. Since fluorine (F) is only available from Nafion and should be constant across the membrane and silicon (Si) is only available from the zeolite nanocrystals, the intensity of F was used as an internal concentration standard, and the Si/F intensity ratio was used to represent the relative quantity of zeolite in the probed region.

Mechanical Property Analysis. The mechanical properties of the membranes were examined under ambient condition with a universal materials testing machine (Instron 5543, Instron Corp.). Stress versus strain plots were generated for the membranes for elongations extending up to failure. Membrane thickness was determined by using a standard metric micrometer with 1 μm resolution.

Raman Spectroscopy. Raman Spectra were recorded using a FT-Raman instrument (Bruker RFS-100/S, Bruker Optics, Inc., 1064 nm) using laser excitation. The power of illumination used was about 200 mW. For pure powdery AFB samples, wafers were prepared by pressing a small amount of AFB powder in an aluminum holder. For the NAFB composite membranes and the Nafion 115 membranes, they were measured by using small pieces of 1 cm × 1 cm size.

Transmission Electron Microscopy (TEM). For the preparation of TEM samples, small pieces of the membranes were first embedded in an epoxy resin ("Spurr" Low Viscosity Kit 18300-4221, Ted Pella, Inc.). The resins were polymerized at 70 °C for 8 h. Samples at a thickness of about 50 nm were microtomed at room temperature using a RMC XT-X and Sorval MT2 ultramicrotome. The thin sections were then examined in a Philips CM 300 transmission electron microscope operated at 200 kV.

Thermoanalysis. A thermogravimetric analyzer (TGA/SDTA851e, Mettler Toledo) was used for the measurement of thermal stability and the AFB nanocrystal loading in the NAFB composite membrane. The thermogravimetric analysis (TGA) data were obtained from 40 °C to 700 °C at a heating rate of 10 °C/min under air flow of 50 mL/min.

Methanol Permeability. The methanol permeability of the composite membranes was determined using the two compartment diffusion cell technique. One compartment (V_A = 62 mL) was filled with a solution of methanol (8 vol %) and 1-butanol (0.2 vol %) in DDI H_2O. The other compartment (V_B = 62 mL) was filled with 1-butanol (0.2 vol %) in DDI H_2O. The membrane (area = 3.14 cm^2) was clamped between the two compartments. The solutions in the two compartments were kept homogeneous using magnetic stir bars at 600 rpm during experiments. Methanol flux was established across the membrane due to the methanol concentration difference between compartment A and compartment B. V_A and

V_B were sufficiently large so that a pseudo-steady-state condition arose after an initial transient period. The methanol concentration in compartment B remained negligible compared to that in compartment A, while the concentration in compartment A remained essentially unchanged during the experiment. Using the above assumptions, methanol flux was constant, and its concentration in compartment B as a function of time is given by $V_B(dC_B/dt) = A(DK/L)C_A$, where C_B is the methanol concentration in compartment B; A is the membrane area; L is the membrane thickness; and D and K are the methanol diffusivity and the partition coefficient between the membrane and the adjacent solution, respectively. The assumptions were made that D was constant inside the membrane and that K did not depend on concentration. P is the membrane permeability and is defined as the product of D and K. C_B was measured several times during the experiment, and the permeability was calculated using the slope of the straight line (C_B versus time), dC_B/dt. A gas chromatograph (SRI 8610C) with a flame ionization detector was used to determine C_B. Samples (2 μL) were drawn from compartment B, and 1-butanol was used as an internal standard for the gas chromatograph.

Proton Conductivity. The proton conductivity of the composite membranes and the Nafion 115 memberanes was measured by a four-electrode method using an AC impedance analyzer under water immersed conditions. A conductivity cell was made up of two platinum foils carrying the current and two platinum wires sensing the potential drop. All the membrane samples were immersed in room-temperature water overnight prior to measurement. The impedance measurements were conducted using an impedance/gain-phase analyzer (Solartron SI 1260) and a potentiostat (Solartron SI 1287). The conductivity of the membrane was calculated using the equation $\sigma = L/RS$, where σ, L, R, and S are the ionic conductivity, distance between the two reference electrodes, resistance of the membrane, and cross-sectional area of the membrane, respectively.

Single DMFC Cell Performance. Electrocatalysts used in the anode and cathode were Pt−Ru/C (80 wt %, Pt:Ru = 1:1, E-TEK) and Pt/C (80 wt %, E-TEK), respectively. The electrodes were prepared according to the following procedure. Both the anode and the cathode consisted of a backing layer, a gas-diffusion layer, and a catalyst layer. Teflon-containing (30 wt % Teflon in cathode, 10 wt % Teflon in anode) carbon papers (EC-TP2-060, ElectroChem, Inc., 190-μm thickness) were employed as backing layers in these electrodes. Teflon 10 wt % for anode and Nafion 20 wt % for cathode in Vulcan XC-72 carbon black was suspended in ethanol and agitated in an ultrasonic water bath, and the slurry was spread onto the carbon paper as gas-diffusion layers (ca. 30-μm thickness). The required amount of catalyst (Pt−Ru/C in the anode, 2.0 mg/cm^2 electrode loading; Pt/C in the cathode, 2.0 mg/cm^2 electrode loading) was mixed with 5 wt % Nafion solution to prepare the catalyst layers, where the dry Nafion loading is 10 wt %. The catalyst ink was coated on the diffusion layer using a spray gun (model H siphon feed single action airbrush, External Mix, Paasche). Finally, a thin layer of 5 wt % Nafion solution was sprayed onto the surface of each electrode (1.0 mg Nafion/cm^2). A MEA with an active electrode area of 5 cm^2 was obtained by pressing the cathode and anode onto each side of a pretreated Nafion 115 membrane or NAFB composite membrane at 140 atm and 135 °C for 3 min (Hydraulic unit model 3912, Carver, Inc.). The MEA was then assembled into a DMFC single cell fixture. The $I-V$ curves were obtained by the following procedure: (1) a single cell was "activated" by 1.0 M or 5.0 M MeOH with 1.0 mL/min for 3 h at 70 °C with no oxygen flow at the cathode at that time; (2) oxygen was introduced and increased until the oxygen pressure reached 0.2 MPa with a flow rate at 0.2 L/min; and (3) the single-cell polarization curves were collected after the operation conditions of the single cell remained stable for 0.5 h. The operation conditions were as follows: anode fuel, 1.0 M or 5.0 M MeOH; flow rate, 1.0 mL/min; no back pressure; oxygen pressure, 0.2 MPa; and flow rate, 0.2 L/min. The temperatures of the cell and cathode humidifier were 70 °C and 65 °C, respectively. All single cell tests were conducted three times, and the results presented here are the average data.

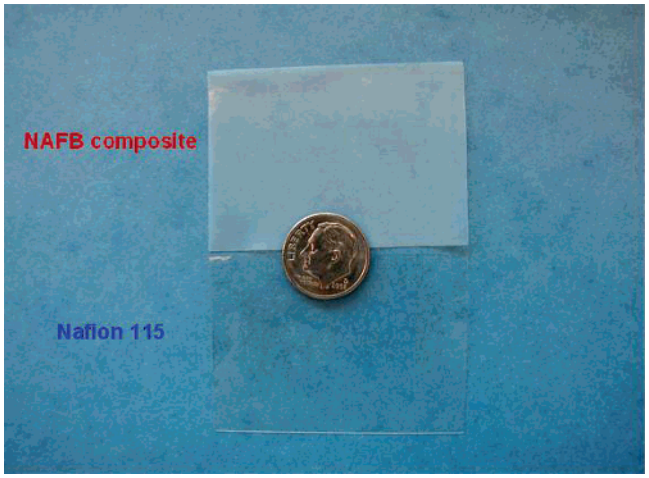

Figure 2. Optical images of NAFB composite membrane and Nafion 115 membrane.

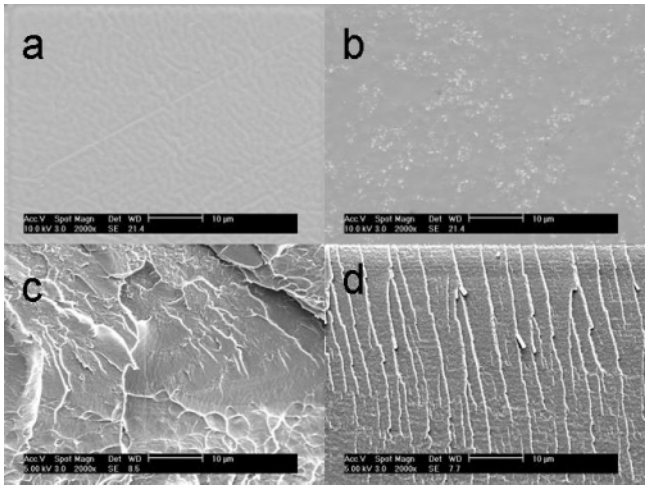

Figure 3. SEM images of the membranes: (a) surface of Nafion 115; (b) surface of NAFB composite; (c) cross-section of Nafion 115; (d) cross-section of NAFB composite.

3. Results and Discussion

Figure 2 shows the optical images of the Nafion 115 and NAFB composite membrane. The Nafion 115 is transparent, but the NAFB composite membrane is cloudy because of the incorporation of AFB nanocrystals. Figure 3 presents the SEM images of the Nafion 115 membrane and the NAFB composite membrane. The surface of Nafion 115 membrane is much smoother than that of the NAFB composite membrane (Figure 3a,b). Particles can be seen on the surface of the NAFB membrane (Figure 3b). However, these particles are not loose zeolite particles. Instead they are likely to be well lodged inside the polymer matrix because the composite membrane has gone through the harsh post-synthesis concentrated sulfuric acid treatment (96 wt % at 80 °C

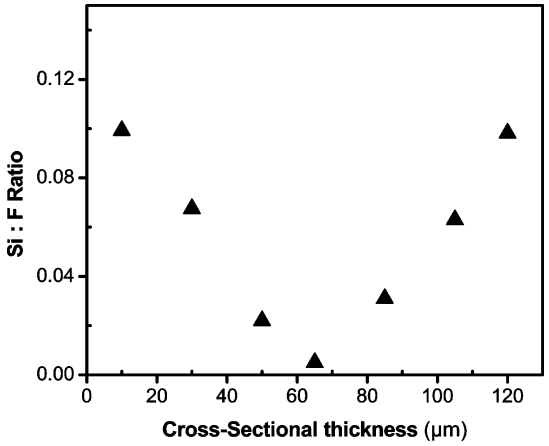

Figure 4. Si/F ratio at different locations within the NAFB composite membrane by EDS/SEM.

overnight). If these crystals are loose ones they would have been removed during the harsh concentrated acid treatment. The cross-sectional images of Nafion 115 and the NAFB composite membrane (Figure 3c,d) show noticeably different appearances, and this may be a reflection of their different mechanical properties.

Since silicon (Si) and fluorine (F) are only available from the AFB nanocrystals and Nafion, respectively, the Si/F ratio can be used to indicate the relative concentration of the AFB nanocrystals inside the membrane (Figure 4). Each point in Figure 4 is the composition within a small area. The Si concentration is higher at the surface and decreases inward from the membrane surfaces with the minimum in the middle, suggesting that the AFB nanocrystals were formed near the surface more than in the internal space of the Nafion membrane.

The cross-sectional TEM images show that the Nafion 115 membrane is uniform and smooth and has no particles at the surface or in the middle (Figure 5a,b). By contrast, the NAFB composite membrane has AFB nanocrystals of (<20 nm) over the entire thickness of the membrane and has more near the surface than in the middle (Figure 5c,d), which is consistent with the elemental analysis results (Figure 4). This is understandable in that the zeolite precursors penetrated into the Nafion membrane through diffusion, and thus a concentration gradient is expected for the precursors and this precursor concentration gradient may have resulted in more and larger crystals near the surface than in the middle the membrane.

The XRD pattern of the Nafion 115 shows two typical peaks at 17° and 40°, while two extra peaks at 7.7° and 22.6° are observed for the NAFB composite membrane (Figure 6). By comparing the positions of these two extra peaks and the two major peaks in the XRD pattern for the pure AFB nanocrystals, it is clear that these two extra peaks are caused by the AFB nanocrystals embedded in the Nafion membranes.

The Raman spectra of the AFB nanocrystals, Nafion 115 membrane, and NAFB composite membrane are shown in Figure 7. The spectrum of the NAFB composite membrane has an extra peak at 1593 cm^{-1} when compared with the Nafion 115 membrane. This peak is a typical peak of the Raman spectrum of AFB nanocrystals,[42,46] which suggests

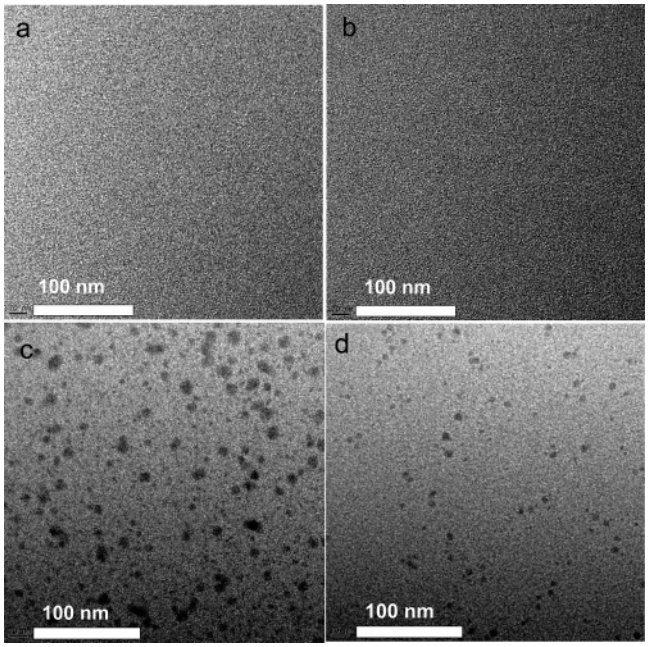

Figure 5. TEM images of the cross sections of the membranes. (a) Nafion 115 near the surface; (b) Nafion 115 in the middle; (c) NAFB composite near the surface; (d) NAFB composite in the middle.

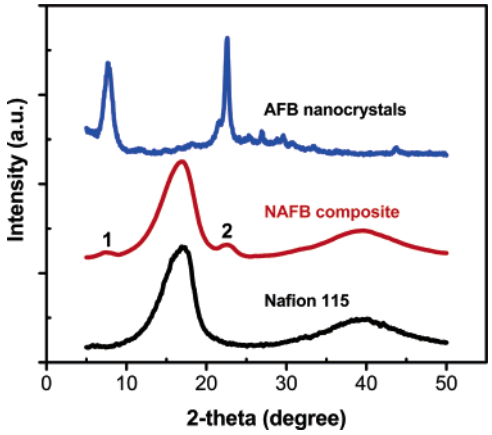

Figure 6. XRD patterns of acid functionalized zeolite Beta nanocrystals, NAFB composite membrane, and Nafion 115 membrane.

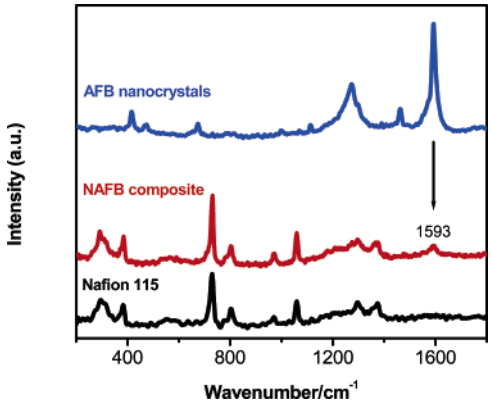

Figure 7. Raman spectra of AFB nanocrystals, NAFB composite membrane, and Nafion 115 membrane.

that AFB nanocrystals are present in the NAFB composite membranes.

Both the composite membranes and the Nafion membranes have good flexibility and mechanical strength. The tensile strength of these two kinds of membranes was measured

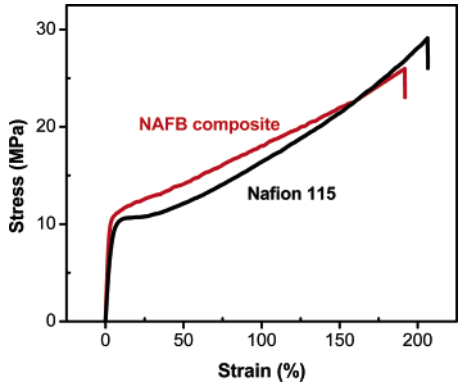

Figure 8. Stress−strain curves of NAFB composite membrane and Nafion 115 membrane.

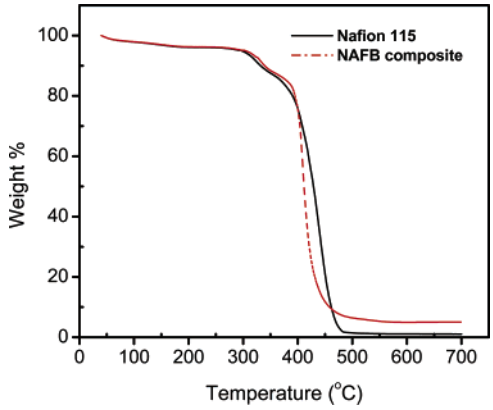

Figure 9. TGA of NAFB composite membrane and Nafion 115 membrane in an air atmosphere with a heating rate of 10 °C/min.

(Figure 8). Although the NAFB composite membrane shows a slightly lower tensile strength than that of the Nafion membrane (25 MPa vs 29 MPa), the Young's modulus (calculated by dividing the tensile stress by the strain) of the composite membrane is much higher than that of Nafion (350 MPa vs 232 MPa).

The thermograms for the Nafion 115 membrane and the NAFB composite membrane are displayed in Figure 9. The samples retain more than 94% weight up to a temperature of about 300 °C. After this point, all samples start decomposing rapidly. It is clear that the incorporation of AFB nanocrystals do not significantly change the thermal stability of the membrane. The AFB loading in the NAFB composite membrane is about 5 wt % because the Beta nanocrystals are still stable at 700 °C.

The proton conductivity and methanol permeability of Nafion 115 and NAFB composite membranes are given in Table 1. The proton conductivity of the NAFB composite membranes is similar to that of Nafion 115 membranes at room temperature. However, its methanol permeability is reduced by 40%. Table 1 also shows the ratio between the proton conductivity and the methanol permeability, an important selectivity factor (ϕ) under this study. The

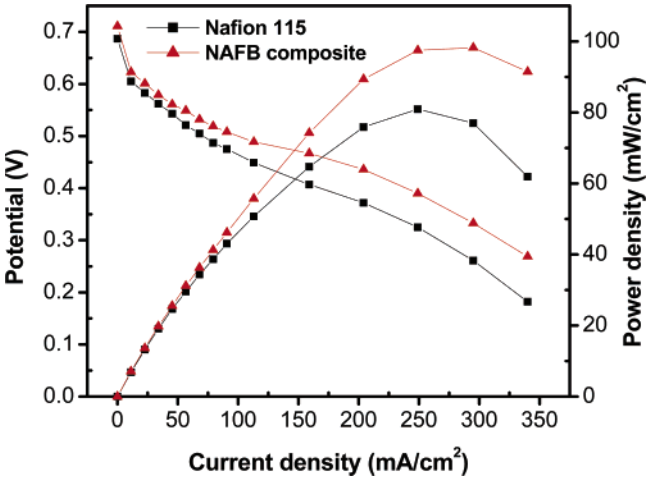

Figure 10. DMFC single cell performance at 70 °C, fed with 1 M CH_3-OH.

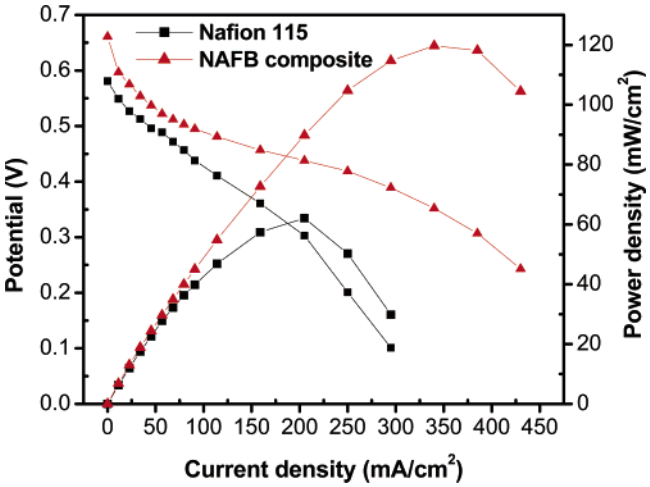

Figure 11. DMFC single cell performance at 70 °C, fed with 5 M CH_3-OH.

selectivity (ϕ) of the NAFB composite membrane is much higher than that of Nafion.

The single cell DMFC performance with the pure Nafion 115 membrane and NAFB nanocomposite membrane using different methanol concentrations (1 and 5 M) at 70 °C is shown in Figures 10 and 11. The DMFC performance for MEAs with the NAFB composite membranes is better than those with the pure Nafion 115 membranes at both methanol concentrations. At the low methanol concentration (1 M MeOH; Figure 10), the DMFC with a NAFB composite membrane shows a higher performance than that with a pure Nafion 115 membrane. The maximum power density is 81 mW/cm^2 for the pure Nafion 115 membrane and 98 mW/cm^2 for the NAFB composite membrane, which is about a 21% increase. When a 5 M methanol concentration is used (Figure 11), the maximum power density of the MEA with the pure Nafion 115 membrane is only 62 mW/cm^2, while the maximum power density of the MEA with the NAFB

Table 1. Proton Conductivity and Methanol Permeability of NAFB Composite Membranes and Nafion 115 at Room Temperature

sample	average thickness (μm) dry	average thickness (μm) wet	average proton conductivity σ (S/cm)	standard deviation of σ	average methanol permeability P (cm^2/s)	standard deviation of P	selectivity $\phi = \sigma/P$ (S s/cm^3)
NAFB	130	151	0.088	0.001	1.40×10^{-6}	6×10^{-8}	6.29×10^4
Nafion 115	127	149	0.091	0.001	2.36×10^{-6}	6×10^{-8}	3.86×10^4

composite is 120 mW/cm^2, which is a 93% increase. Comparing the same membrane DMFC performance at different methanol concentration (1 M compared to 5 M), the maximum power density was increased by 22% for the NAFB composite membrane, but it decreased by 24% for the pure Nafion 115 membrane. The open circuit voltage (OCV) of a MEA is closely related to the methanol crossover. Higher methanol crossover leads to a lower OCV. In Figures 10 and 11, the OCVs of the NAFB composite membrane and the pure Nafion 115 decreased with increasing methanol concentration, but the OCVs of the NAFB composite membranes were higher than that of the pure Nafion 115 membranes under both 1 M and 5 M methanol conditions. When 1 M methanol was used, the MEA with NAFB composite membrane had a slightly (3%) higher OCV (0.71 V) than the pure Nafion 115 membrane (0.69 V; Figure 10). However, with a 5 M methanol feed, a 14% higher OCV was achieved for the NAFB composite membrane (0.64 V vs 0.58 V; Figure 11). The higher OCV indicates that AFB nanocrystals embedded into the Nafion membrane have greatly decreased the rate of methanol crossover. The higher maximum power density indicates a better performance of NAFB composite membrane than that of the pure Nafion membrane. The results also suggest that fuel with a high concentration of methanol can be used in a DMFC by using the NAFB composite membrane.

4. Conclusions

NAFB nanocomposite membranes have been successfully prepared by an in situ hydrothermal crystallization method. The AFB nanocrystals are estimated to have a diameter less than 20 nm, and their loading in the membrane is 5 wt %. Compared with the commercial Nafion membrane, the composite membrane has similar proton conductivity but much lower methanol permeability (40% reduction). The NAFB composite membrane has a slightly higher OCV (3%) and much higher maximum power density (21%) than that of the pure Nafion with a 1 M methanol feed. At a higher methanol concentration (5 M), the performance of the DMFC with NAFB composite membrane shows a 14% higher OCV and a 93% higher maximum power density than the Nafion 115 membranes. The NAFB composite membranes have the potential to allow use of fuel with high methanol concentrations. The in situ hydrothermal crystallization method also can be used to impregnate other zeolite nanocrystals into Nafion and other polymer membranes.

Acknowledgment. The authors gratefully acknowledge the U.S. National Science Foundation (NSF) (CTS-0404376), the U.S. Department of Energy (DE-FG02-05ER15716), and the Riverside Public Utilities for their financial support and E-TEK for generously donating the Pt/C and PtRu/C catalysts.

CM060841Q